Int. J. Solids Structures Vol. 24, No. 3, pp. 231–250, 1988
Printed in Great Britain.

0020–7683/88 $3.00 + .00
Pergamon Press plc

MICROCRACK COALESCENCE AND MACROSCOPIC CRACK GROWTH INITIATION IN BRITTLE SOLIDS

M. ORTIZ
Division of Engineering, Brown University, Providence, RI 02912, U.S.A.

(*Received* 3 *December* 1986; *in revised form* 7 *July* 1987)

Abstract—The problem studied in this paper concerns the analytical estimation of the effect of microcracking on crack growth initiation in brittle solids. Particular attention is given to the counteracting effects of toughness degradation and shielding by macrocracking, with a view to determining the range of dominance of each mechanism. Crack growth initiation by coalescence with microcracks is studied with the aid of a cohesive zone model. The extent of shielding of the crack tip by the intervening microcracks is estimated under isotropic damage conditions. A comparison of these effects reveals that, were the crack capable of growing within its plane, the toughness enhancement derived from shielding would be almost exactly counterbalanced by the reduction of toughness in the microcracked material. However, if microcrack deflection is taken into account levels of toughening consistent with experimental data are computed.

1. INTRODUCTION

The problem studied in this paper concerns the analytical estimation of the effect of microcracking on crack growth initiation in brittle solids. A growing body of observational evidence attributes a dual role to microcracking in relation to fracture of brittle materials such as ceramics and rocks. On one hand microcracking is thought to contribute to the stability of macroscopic cracks by softening the material surrounding the tip, thereby mitigating the effect of the applied loads[1, 2]. On the other hand, the microcracks created ahead of the main crack can be expected to reduce the resistance to fracture of the material. The next extent of toughening or embrittlement is the result of the counteracting effects of shielding and degradation.

For microcracking to provide effective shielding, it is critical that microcracks remain stable following nucleation. In ceramics and rocks, this is accomplished by microcracks forming at grain boundary facets and remaining confined to them thereafter. Under increasing loads the number of available nucleation sites is eventually exhausted and the material asymptotically attains some reduced elastic moduli. The presence of softer material around the crack tip has the effect of screening the remote loads, thereby reducing the level of stress. Furthermore, newly formed microcracks partially relieve residual stresses that develop in the material during cooling. This process manifests itself on the macroscopic scale as a transformation strain[3, 4] and constitutes another source of toughening. Ultimately, the crack advances by coalescence with microcracks ahead of the tip, a mechanism which is promoted by profuse microcracking. Further microstructural background on microcrack shielding and crack growth initiation can be found in Refs [5–7].

Earlier studies of this problem focused mainly on the toughening effect of microcracking[3, 8–12]. A principal objective of these analyses is to establish a relation between the stress intensity factor at the crack tip K_t and the amplitude K_∞ of the surrounding K-field, or "applied" stress intensity factor. The extent to which K_t is reduced below K_∞ provides a quantitative measure of shielding. A material which nucleates microcracks normal to the direction of maximum tensile stress was considered in Ref. [12], where a closed form expression for K_t/K_∞ for a stationary crack was derived. The analysis given in Ref. [3] takes transformation strains into consideration and was carried out for both stationary and steady growth conditions. A noteworthy outcome of this work is the observation that anisotropic microcracking screens the applied loads more effectively than isotropic damage.

By contrast, relatively little attention has been given to the problem of estimating the inherent fracture toughness of a microcracked material. In this paper, a model is discussed that seeks to describe, albeit approximately, the process of crack growth initiation by coalescence with microcracks. The microcracks which weaken the material ahead of the main crack are regarded as introducing a cohesive zone of the type originally proposed by

Dugdale[13] and Barenblatt[14] for plane stress yielding. An effective cohesive stress-opening displacement relation is obtained by means of a homogenization argument. In this way, a number of results and methods from elastic–plastic fracture mechanics can be brought to bear on the problem under consideration. In particular, the toughness of the microfractured material can be determined as a function of the density of microcracks.

Some limitations of the present approach should be noted. The Dugdale zone technique has been used in other similar studies. For instance, Budiansky[15] idealized the effect of bridging particles in a ceramic material as a smeared cohesive zone. As in the present work, the effective behavior of the bridging zone was determined by recourse to a homogenization argument involving averages over large numbers of particles. However, one finds *a posteriori* that the estimated size of the cohesive zone only includes a reduced number of bridging particles. In spite of this limitation, the cohesive zone approximation does seem to capture the relevant features of the bridging mechanism[15]. In the present case, it is also found that strong interactions with the main crack are confined to the first few leading microcracks during most of the separation process. However, as the moment of coalescence is neared, an increasing number of microcracks appears to become involved. Thus, the homogenization argument on which the present analysis is predicted may be expected to be most appropriate at coalescence, i.e. at the moment of primary interest. Nevertheless, the localized nature of the interactions points to a direct analytical treatment of a small number of microcracks as a likely improvement over the present method. In addition to the above approximations, the problem is idealized as being two-dimensional with the main crack growing self-similarly by coalescence with slit cracks. Here again, simplifying assumptions of a similar nature pervade most of the literature on both brittle and ductile crack growth. These idealizations may be expected to overestimate somewhat the extent of toughness degradation.

The remaining part of this paper aims at weighing the relative influence of shielding and degradation on fracture toughness. To facilitate comparison of results we focus on shielding by isotropic damage, the pertinent features of which are given a succinct derivation in Section 3. The main result of this section is a closed form expression for K_I/K_∞ which is not restricted to dilute concentrations of microcracks. From these estimates it is possible to derive some theoretical insight into the relative roles played by the various competing micromechanisms, as discussed in Section 4.

2. WEAKENING EFFECT OF MICROCRACKS AHEAD OF A MAIN CRACK

In this section we concern ourselves with the problem of quantifying the deleterious effect of microcracking on fracture toughness. For cracks in the materials considered here, extensive microcracking occurs within a certain zone surrounding the crack tip. The presence of a microcracked region facilitates crack growth by coalescence with microcracks, thus having a detrimental effect on fracture toughness. The characteristic length scale of this process is furnished by the spacing between microcracks. This distance is typically of the order of several grain sizes and will be herein assumed to be much smaller than the length of the macrocrack. Under these conditions, the main crack can be regarded as being semi-infinite, an idealization which is adopted throughout in the analysis that follows.

2.1. *A cohesive zone model*

To make the problem tractable, we resort to the following simplifying assumptions. The weakening effect of microcracking is taken into account by considering a collinear array of uniformly spaced microcracks lying within the plane of the main crack (Fig. 1(a)). Collinear microcrack models have been used in the past to estimate the tensile strength of ceramics[16–18]. The material surrounding the crack tip is treated as a linear elastic body endowed with the effective moduli of the homogenized continuum. For simplicity, these are assumed to remain isotropic throughout the process of loading. In this paper, attention will be confined to plane strain crack problems in which the remote loads are symmetric with respect to the crack (Mode I). Under these conditions, the main crack and trailing microcracks will open symmetrically and grow within their plane (Fig. 1(a)).

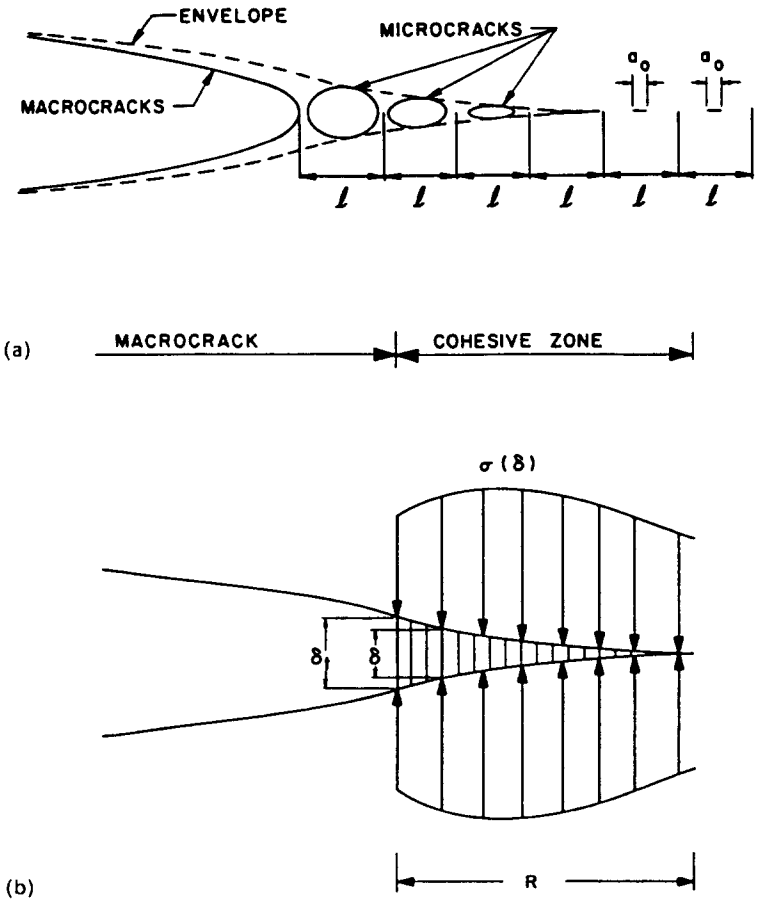

Fig. 1. (a) Semi-infinite crack weakened by an array of microcracks. (b) Cohesive zone idealization.

To simplify the analysis further, the array of microcracks is modelled as a cohesive zone of the type introduced by Dugdale[13] and Barenblatt[14] (Fig. 1(b)). The traction-opening displacement within the cohesive zone is determined by means of the following homogenization argument. Consider an infinite array of uniformly spaced collinear microcracks of equal length in an unbounded isotropic elastic body subjected to a remote traction σ (Fig. 2). An analytical solution to this problem has been given by Koiter[19]. A

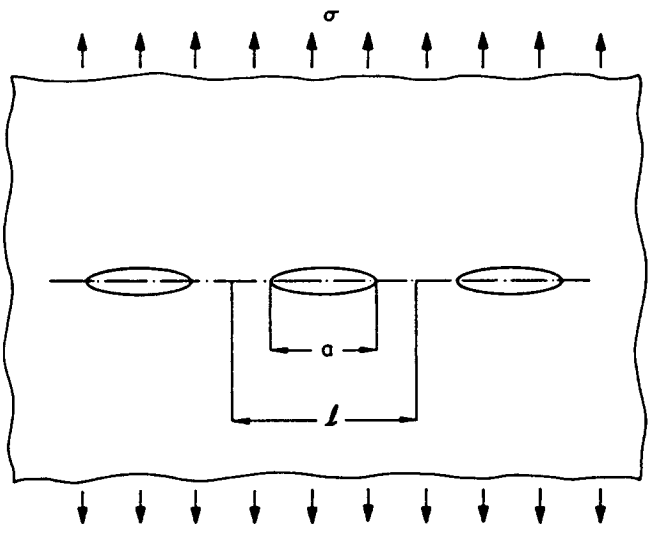

Fig. 2. Model problem for obtaining the effective properties of the cohesive zone.

feature of the solution which bears directly on the problem at hand is the increase in strain energy per microcrack, which is given by

$$W_1 = -\sigma^2 \frac{8l^2}{\pi} \frac{1-\nu^2}{E} \log \cos \frac{\pi a}{2l}. \tag{1}$$

Here, $2l$ is the spacing between the microcracks, $2a$ is the size of the cracks and E and ν are Young's modulus and Poisson's ratio of the material, respectively. Passage to the continuum limit can be accomplished in the usual fashion. Consider an interval Δx in the plane of the cracks. If Δx is much larger than l, the increase in strain energy due to the cracks within the interval is given to a good approximation by

$$\Delta W \approx W_1 \frac{\Delta x}{2l} = -\sigma^2 \frac{4l}{\pi} \frac{1-\nu^2}{E} \log \cos \frac{\pi a}{2l} \Delta x. \tag{2}$$

Hence, the strain energy U per unit length of the plane of the cracks is computed to be

$$U \equiv \frac{\Delta W}{\Delta x} \approx -\sigma^2 \frac{4l}{\pi} \frac{1-\nu^2}{E} \log \cos \frac{\pi a}{2l}. \tag{3}$$

The effective opening displacement δ of the array of cracks is defined as the variable work conjugate to σ, i.e.

$$\delta = \frac{\partial U}{\partial \sigma} = -\sigma \frac{8l}{\pi} \frac{1-\nu^2}{E} \log \cos \frac{\pi a}{2l}. \tag{4}$$

This expression establishes a linear relation between the remote traction σ and the opening displacement δ. Introducing the stiffness k of the weakened plane as

$$\delta = \frac{\sigma}{k} \tag{5}$$

one has from eqn (4)

$$k = -\frac{\pi}{8l} \frac{E}{1-\nu^2} \Big/ \log \cos \frac{\pi a}{2l}. \tag{6}$$

Note the strong dependence of k on the microcrack size (Fig. 3(a)). In particular, k is seen to decrease to zero as the cracks coalesce, i.e. as a approaches l.

The array of microcracks ahead of the main crack is now modelled as a cohesive zone obeying pointwise the traction-displacement law expressed in eqn (4). In this context, l is presumed known and a/l, σ and δ are to be interpreted as the pointwise values of the microcrack density, normal traction and opening displacement on the plane of the crack, respectively. At points sufficiently distant from the crack tip the microcrack size is assumed to be uniform and equal to a_0. As the crack tip is approached, the microcrack size can be expected to increase steadily. To determine the distribution of microcrack sizes within the cohesive zone we postulate the microcrack growth criterion

$$K_I \leqslant K_{IC}^0 \tag{7}$$

where K_I is the local stress intensity factor at the tip of the microcracks and K_{IC}^0 is the toughness of the uncracked material. For an infinite array of collinear cracks, the value of K_I was computed by Rice[20] to be

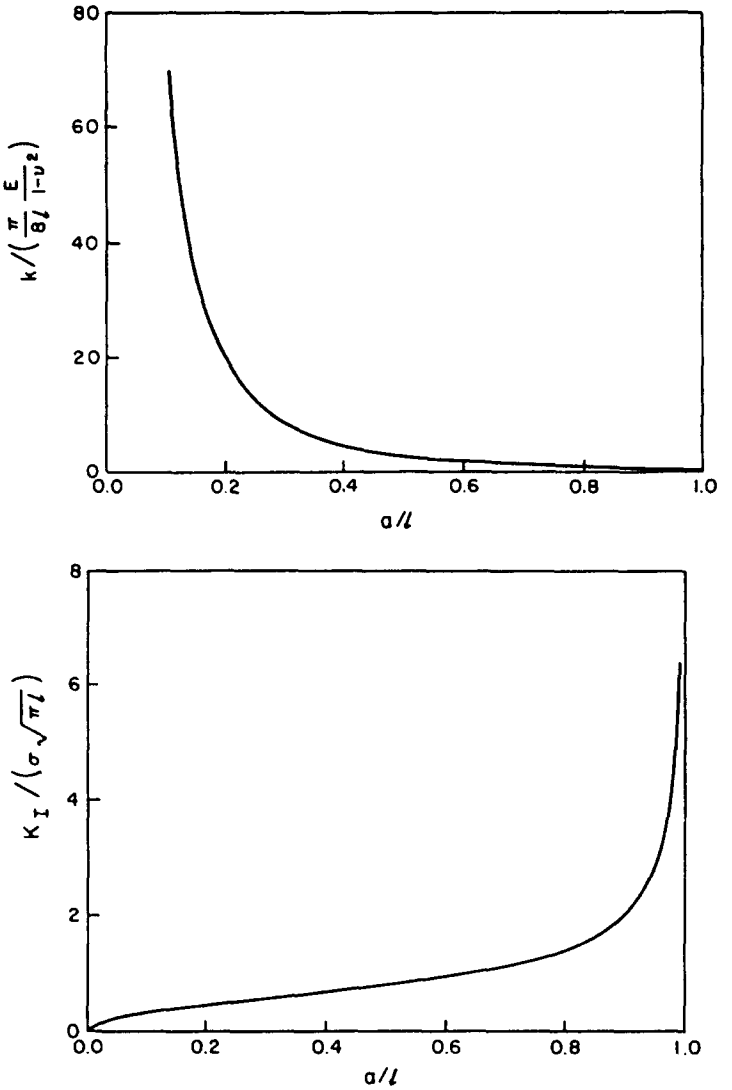

Fig. 3. Effective stiffness k of cohesive zone and microcrack stress intensity factor K_I as a function of microcrack size.

$$K_I = \sigma\sqrt{(\pi l)}\sqrt{\left(\frac{2}{\pi}\tan\frac{\pi a}{2l}\right)}. \tag{8}$$

The dependence of K_I on the microcrack size is shown in Fig. 3(b). A noteworthy feature of this dependence is that K_I grows unboundedly as the microcracks coalesce, i.e. as $a \to l$.

Equations (4) and (8) combined suffice to determine the effective behavior of the cohesive zone. For values of δ in the interval

$$0 < \delta \leqslant \delta_0 = \frac{\sigma_0}{k_0} \tag{9}$$

where

$$\sigma_0 = \frac{K_{IC}^0}{\sqrt{(\pi l)}}\Big/\sqrt{\left(\frac{2}{\pi}\tan\frac{\pi a_0}{2l}\right)}, \quad k_0 = -\frac{\pi}{8l}\frac{E}{1-\nu^2}\Big/\log\cos\frac{\pi a_0}{2l} \tag{10}$$

K_I remains below K_{IC}^0 and the traction–displacement relation takes the linear form

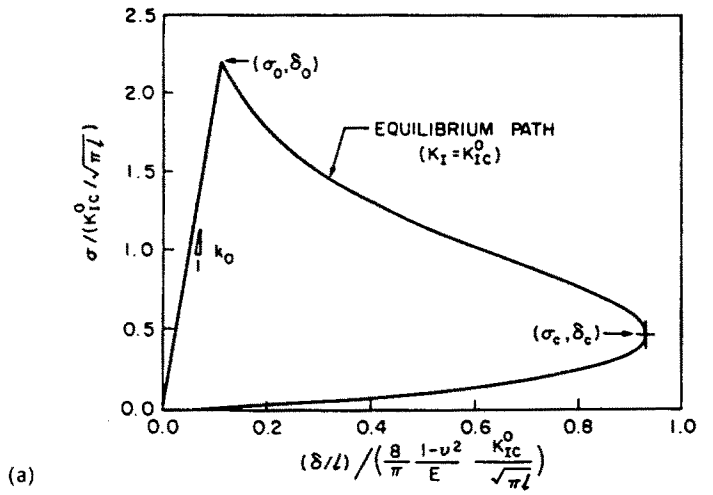

(a)

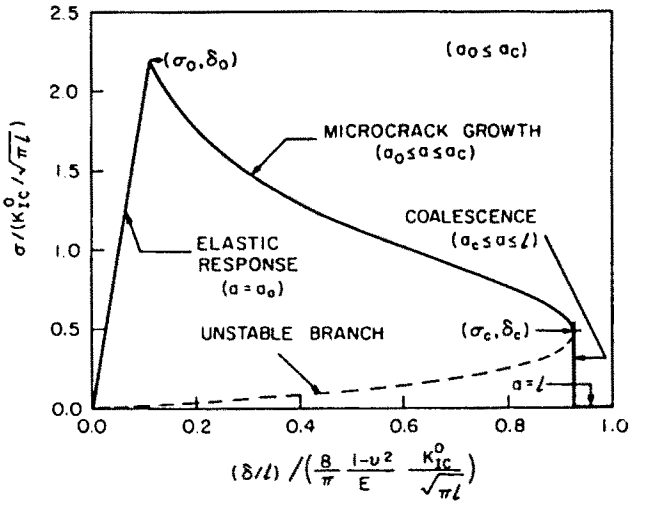

(b)

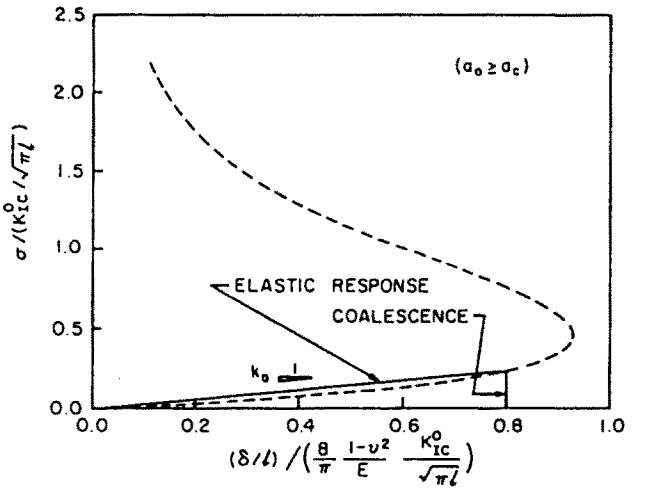

(c)

Fig. 4. (a) Equilibrium traction opening displacement relation within cohesive zone. Effective traction–opening displacement relation taking microcrack coalescence into consideration; (b) subcritical initial microcrack size; (c) supercritical initial microcrack size.

$$\delta = \frac{\sigma}{k_0}. \tag{11}$$

When threshold (9) is exceeded, microcracks grow in order to satisfy inequality (7). Figure 4(a) shows the traction–displacement law obtained by assigning values to a in the

interval $[a_0, l)$, and the computing k from eqn (6), σ from eqn (8) with $K_I = K_{IC}^0$ and finally δ from eqn (5). A striking feature of the equilibrium path is that it becomes unstable at

$$\sigma_c \approx 0.4727 \times \frac{K_{IC}^0}{\sqrt{(\pi l)}}, \quad \frac{\delta_c}{l} \approx 0.9266\alpha, \quad \alpha \equiv \frac{8}{\pi}\frac{1-\nu^2}{E}\frac{K_{IC}^0}{\sqrt{(\pi l)}}. \tag{12}$$

This corresponds to a microcrack density

$$\frac{a_c}{l} \approx 0.91. \tag{13}$$

Beyond this point microcrack growth cannot be sustained statically at constant K_{IC}. Opening beyond δ_c results in cleavage of the ligaments between the microcracks. Although this process is inherently dynamic, the transient response is herein ignored and the stress σ is assumed to drop instantaneously to zero following coalescence. The resulting traction–displacement law is shown in Fig. 4(b). As can be seen, following an initial elastic range $(0, \delta_0)$, a softening response is obtained in the interval (δ_0, δ_c), beyond which the microcracks coalesce and the stress drops to zero. In the preceding discussion it has been tacitly assumed that the initial microcrack density a_0/l is below the critical value a_c/l. If the opposite is true, the effective behavior is as shown in Fig. 4(c), i.e. the microcracked zone behaves linearly up to coalescence, henceforth losing its bearing capacity.

2.2. *Fracture toughness of the microcracked solid*

By virtue of the above formulation, a number of results concerning cohesive zone models can be brought to bear on the problem at hand. Of primary interest is to determine conditions under which crack growth will initiate. Such conditions follow simply from an application of the J-integral of Rice[20]. A classical result[20] shows that the path-independent value of J is given by

$$J = \int_0^{\delta_t} \sigma(\delta)\, \mathrm{d}\delta \tag{14}$$

where δ_t signifies the crack tip opening displacement (Fig. 1(b)) and $\sigma(\delta)$ is the effective traction–displacement law depicted in Figs 4(b) and (c). Crack extension becomes possible at loads large enough to elevate J to a value corresponding to $\delta_t = \delta_c$, i.e.

$$J = J_{IC} = \int_0^{\delta_c} \sigma(\delta)\, \mathrm{d}\delta. \tag{15}$$

For the traction–displacement law derived above, one finds

$$J_{IC} = \frac{1-\nu^2}{E}(K_{IC}^0)^2 f\left(\frac{\pi a_0}{2l}\right) \tag{16}$$

where the dimensionless function f reads

$$f(\theta) = 1.0876 - \frac{4}{\pi}\left[\theta - \arctan\left(\frac{\sin\theta}{\cos\theta + 1}\right)\right]. \tag{17}$$

A derivation of this expression is given in Appendix A.

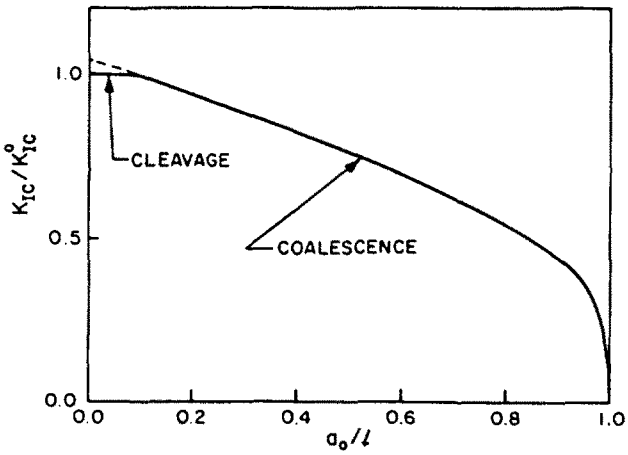

Fig. 5. Reduction in inherent toughness of microcracked material as a function of microcrack size.

At large distances from the cohesive zone the deformation and stress fields can be expected to be indiscernible from the elastic solution. Thus, computation of J from a contour sufficiently removed from the crack tip yields the classical result

$$J_t = \frac{1-\nu^2}{E} K_t^2 \tag{18}$$

where K_t is the amplitude of the surrounding K-field. The toughness K_{IC} of the material can be identified with the value of K_t which renders $J_t = J_{IC}$. The J-integral being path independent, it follows from eqns (15) and (18) that

$$\frac{K_{IC}}{K^0_{IC}} = \sqrt{\left(f\left(\frac{\pi a_0}{2l}\right)\right)}. \tag{19}$$

Surprisingly, K_{IC}/K^0_{IC} is seen to be independent of the elastic properties of the material and to depend solely on the microcrack density a_0/l. This dependence is shown in Fig. 5, where the detrimental effect of microcracking is clearly apparent. For values of $a_0/l < 0.08$, the effective toughness predicted by eqn (19) is greater than K^0_{IC}. Thus, for small microcrack densities crack growth by cleavage at K^0_{IC} can be expected to prevail over microcrack coalescence.

The size of the cohesive zone can be estimated from standard results. To this end, let us approximate the traction–displacement law by a step function (Fig. 6(a)). The average stress $\langle\sigma\rangle$ displayed in Fig. 6(a) is chosen so as to match the area under the original traction–displacement curve, i.e. $\langle\sigma\rangle \equiv J_{IC}/\delta_c$. Then, a classical computation[20] reveals that for a material obeying the step function law the size R of the cohesive zone at crack growth initiation is given by

$$\frac{R}{l} = \frac{\pi}{8l}\frac{K_{IC}^2}{\langle\sigma\rangle^2} \approx 0.6959 \Big/ f\left(\frac{\pi a_0}{2l}\right). \tag{20}$$

The dependence of R on the parameters involved is shown in Fig. 6(b). From this estimate it may be concluded that strong interactions with the main crack are confined to the first few leading microcracks during most of the separation process. However, as the moment of coalescence is neared, an increasing number of microcracks appears to become involved. Thus, the homogenization argument on which the present analysis is based may be expected to be most accurate as coalescence is approached. Nevertheless, the localized nature of the interactions points to a direct analytical treatment of a small number of microcracks as a likely improvement over the present method.

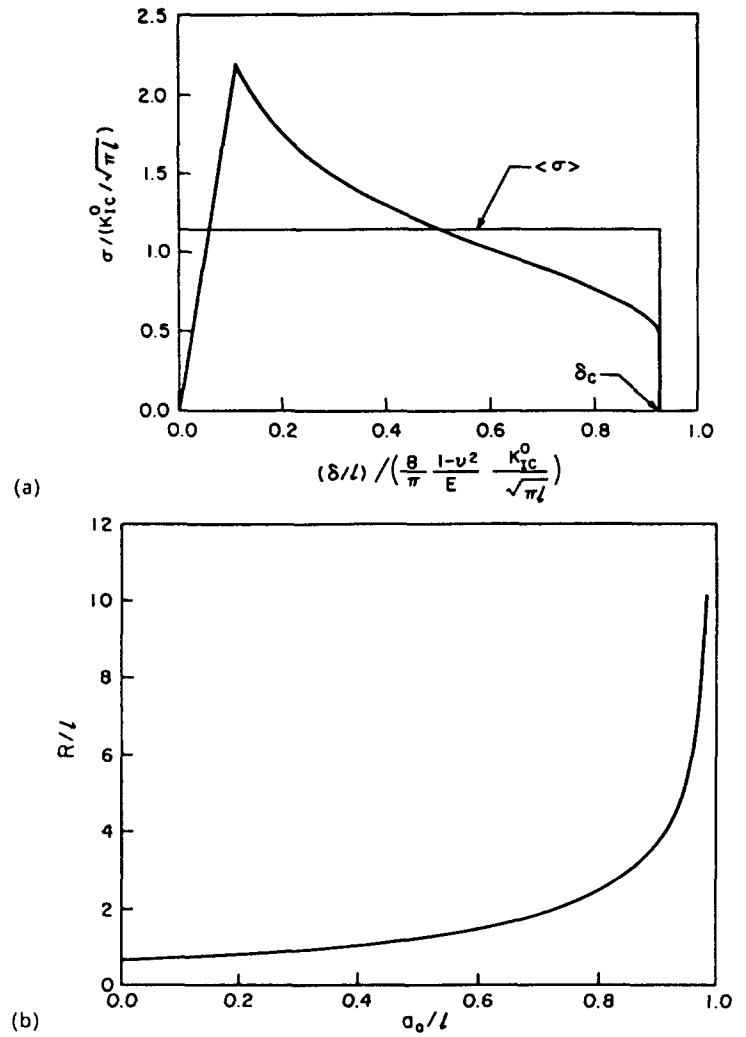

Fig. 6. (a) Average cohesive stress used to estimate the size of the cohesive zone. (b) Size of cohesive zone as a function of microcrack size.

3. MICROCRACK SHIELDING

In this section we turn our attention to the microcrack shielding mechanism. We take the viewpoint that both the size of the microcracks and their separation are small with respect to the dimensions of the microcracked region. Under these conditions, a typical material element can be regarded as containing numerous microcracks and the calculations may be based on the effective behavior of the homogenized solid. We begin the section with a brief discussion of some aspects of the mechanics of microcracked solids which have a direct bearing on the problem under consideration. The simplifying assumption is made that the solid remains ostensibly isotropic after microcracking. This supposition is introduced with a view to facilitating comparisons with the results of the previous section, which strongly rely on isotropy. An analysis of microcrack shielding which accounts for induced anisotropy is given in Ref. [12].

Of primary concern in formulating constitutive equations for the microcracked solid is that they properly reduce to a deformation theory for monotonic stress paths. For stationary cracks, the stresses at every material point can be reasonably expected to remain nearly proportional if the loads are increased monotonically. Under these conditions and provided that the aforementioned constitutive restriction is satisfied, the behavior of the material becomes indistinguishable from that of a non-linear elastic solid and Rice's J-integral applies. This permits one to compute the shielding ratio K_t/K_∞ in closed form for arbitrary extents of damage.

3.1. *Incremental isotropic damage*

Under the simplifying assumption that the body remains isotropic at all times, the state of microcracking can be characterized by means of a scalar internal variable q. For instance, using a self-consistent method Budiansky and O'Connell[21] computed the effective moduli of a solid containing randomly distributed circular microcracks to be

$$\begin{aligned}\frac{\bar{E}}{E} &= 1-\frac{16}{45}\frac{(1-\bar{\nu}^2)(10-3\bar{\nu})}{2-\bar{\nu}}q\\ \frac{\bar{G}}{G} &= 1-\frac{32}{45}\frac{(1-\bar{\nu})(5-\bar{\nu})}{2-\bar{\nu}}q\\ q &= \frac{45}{16}\frac{(\nu-\bar{\nu})(2-\bar{\nu})}{(1-\bar{\nu}^2)[10\nu-\bar{\nu}(1+3\nu)]}\end{aligned} \tag{21}$$

where $\bar{E}$, $\bar{G}$ and $\bar{\nu}$ denote the effective Young's modulus, shear modulus and Poisson's ratio, respectively. Here q provides a measure of microcrack density and is given by $q = N\langle r^3\rangle$, where N is the number of microcracks per unit volume, r is the radius of the microcracks and the angular brackets denote an average. The corresponding complementary energy of the solid can be written as

$$\chi(\sigma, q) = \frac{1}{2}\left(\frac{p^2}{\bar{K}} + \frac{s_{ij}s_{ij}}{2\bar{G}}\right) \tag{22}$$

where $p = \sigma_{kk}/3$ is the hydrostatic pressure, $s_{ij} = \sigma_{ij} - p\delta_{ij}$ the stress deviator and $\bar{K} = \bar{E}/3(1-2\bar{\nu})$ is the effective bulk modulus. The function χ furnishes a Gibbs potential for the strains in the sense that

$$\varepsilon_{ij} = \frac{\partial\chi(\sigma, q)}{\partial\sigma_{ij}}. \tag{23}$$

Guided by these results, we direct our attention to materials the Gibbs function χ of which exhibits an arbitrary dependence on the state variables (σ, q), where q denotes some suitable damage parameter. The corresponding stress–strain relation is still given by eqn (23). To complete the description of the material, an equation of evolution needs to be specified for q. If rate effects are neglected, this can be accomplished by postulating a microcrack nucleation criterion. Here, we focus on criteria of the type

$$F(Q(\sigma, q)) = Q_c(q) \tag{24}$$

where F and Q_c are scalar functions and

$$Q = \frac{\partial\chi(\sigma, q)}{\partial q} \tag{25}$$

is the thermodynamic force conjugate to q. From this viewpoint, Q_c can be regarded as a critical value of Q for nucleation. The assumption implicit in eqn (25) is that the evolution of q depends on the state variables (σ, q) only through the conjugate force $Q(\sigma, q)$. Arbitrary as it may seem at this point, this postulate is critical for the J-integral formalism to apply, as discussed in Section 3.2.

Suitable loading–unloading conditions can be formulated in Kuhn–Tucker form as the requirement that the constraints

$$F(Q(\sigma, q)) - Q_c(q) \leqslant 0, \quad \dot{q} \geqslant 0, \quad [F(Q(\sigma, q)) - Q_c(q)]\dot{q} = 0 \tag{26a–c}$$

be simultaneously satisfied at all times. Inequality (26a) embodies the nucleation criterion, (26b) expresses the irreversibility of damage and (26c) necessitates that eqn (24) be satisfied whenever $\dot{q} > 0$ and that $\dot{q} = 0$ whenever $F(Q(\sigma, q)) - Q_c(q) < 0$.

For this simple class of models the dependence of Q_c on q can be entirely determined from the uniaxial stress–strain curve, a situation which is reminiscent of isotropic plasticity. We illustrate this point for the simple case of potential (22). Let $\varepsilon(\sigma)$ denote the stress–strain law under monotonically increasing uniaxial tension. From the relation

$$\sigma = \bar{E}(q)\varepsilon(\sigma) \tag{27}$$

we can solve for σ as a function of q. On the other hand, particularizing definition (25) to uniaxial conditions we obtain

$$Q = \frac{\bar{E}'(q)\sigma^2}{2\bar{E}^2(q)}. \tag{28}$$

Finally, combining eqns (27) and (28) and noting that the nucleation criterion (26) is identically satisfied throughout the loading process we conclude that

$$Q_c(q) = F\left(-\frac{\bar{E}'(q)\sigma^2(q)}{2\bar{E}^2(q)}\right) \tag{29}$$

which expresses the sought dependence of Q_c on the internal parameter q.

For the class of materials under consideration, the uniaxial stress–strain curve is taken to be of the form shown in Fig. 7(a). The rationale behind this assumption is the following. Below a critical stress σ_0, the elastic moduli can be expected to remain constant and equal to the uncracked moduli, E_0, ν_0. Beyond this threshold, microcracks are assumed to nucleate at grain boundary facets where they arrest and remain stable thereafter. Thus, damage to the material accumulates as a result of additional nucleation sites being activated and not by extension of already existing microcracks. Consequently, as the fraction of nucleation sites which are favorably oriented with respect to the loading axes is exhausted, a saturation stage sets in, say at stress σ_s, beyond which the effective moduli E_s and ν_s remain unchanged. Eventually, microcracks start to coalesce and the present description ceases to be adequate.

The precise form of the transition range between σ_0 and σ_s is immaterial to the present analysis, as long as the nucleation criterion is of the form of eqn (24). By contrast, the postulated existence of a saturation stage is strongly relied upon. Although the observational evidence remains scarce, the assumption of a well-defined saturation state pervades most previous work to date. A more realistic constitutive description allows for an offset strain ε^r in the saturated branch of the stress–strain law (Fig. 7(b)). The strain ε^r is due to release of local residual stresses, and can be thought of as a transformation strain[3]. There is no difficulty in extending the above constitutive framework to take this effect into account. However, in the context of crack growth initiation transformation strains may be reasonably expected to play a negligible role. Thus, on one hand, their magnitude is estimated to be relatively small in materials such as alumina[4]. Furthermore, transformation strains remain bounded under increasing stress and are thus overwhelmed by the stress-proportional part of the deformation as the crack tip is approached. In view of these observations, transformation strains are neglected throughout the calculations that follow. By way of contrast, it should be noted that transformation strains may be of considerable significance in the context of steady crack growth.

3.2. *Associated deformation theories*

Next we seek to characterize the constitutive response predicted from the general theory under monotonic loading conditions. For stress paths such that

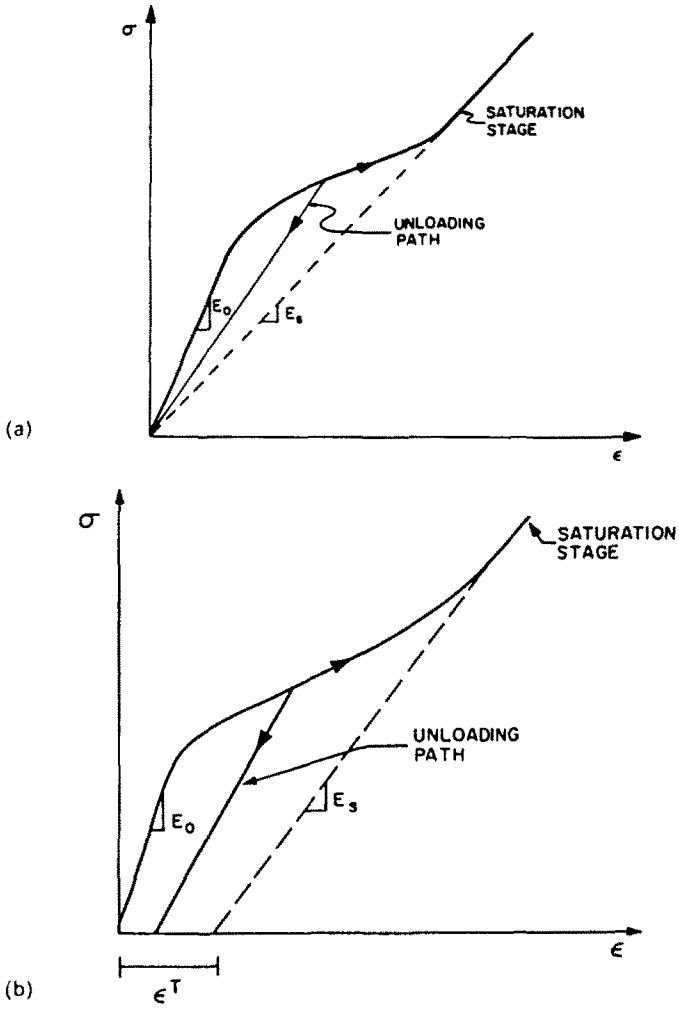

Fig. 7. Characteristic tensile stress strain curves: (a) without transformation strain; (b) with transformation strain ε^{T}.

$$\dot{Q}(\sigma, q) = \frac{\partial Q}{\partial \sigma_{ij}} \dot{\sigma}_{ij} + \frac{\partial Q}{\partial q} \dot{q} \geqslant 0 \tag{30}$$

at all times, nucleation criterion (24) is identically satisfied and one can solve for q as a function of σ. This yields a relation

$$q = g(\sigma) \tag{31}$$

where the function g is determined from the condition

$$F[Q(\sigma, g(\sigma))] = Q_c(g(\sigma)). \tag{32}$$

Substituting eqn (31) into eqn (23) one obtains

$$\varepsilon_{ij} = \frac{\partial \chi}{\partial \sigma_{ij}}(\sigma, g(\sigma)) \equiv \varepsilon_{ij}(\sigma). \tag{33}$$

Thus, under monotonic stressing in the sense of eqn (30) the constitutive response is indistinguishable from that of a hypoelastic material with stress–strain relations $\varepsilon(\sigma)$. A question of primary importance for the applicability of the J-integral is to determine sufficient conditions for $\varepsilon(\sigma)$ to derive from a potential, i.e.

$$\varepsilon_{ij}(\boldsymbol{\sigma}) = \frac{\partial \Omega(\boldsymbol{\sigma})}{\partial \sigma_{ij}} \tag{34}$$

for some $\Omega(\boldsymbol{\sigma})$. The integrability conditions for eqn (34) are

$$\frac{\partial \varepsilon_{ij}(\boldsymbol{\sigma})}{\partial \sigma_{kl}} = \frac{\partial \varepsilon_{kl}(\boldsymbol{\sigma})}{\partial \sigma_{ij}}. \tag{35}$$

But from eqn (33) it follows that

$$\frac{\partial \varepsilon_{ij}}{\partial \sigma_{kl}} = \frac{\partial^2 \chi}{\partial \sigma_{ij}\partial \sigma_{kl}} + \frac{\partial^2 \chi}{\partial \sigma_{ij}\partial q}\frac{\partial f}{\partial \sigma_{kl}}. \tag{36}$$

Thus, a necessary and sufficient condition for the existence of a potential is that the second term on the right-hand side of eqn (36) be symmetric. This question can be decided with the aid of eqn (32). Differentiating with respect to $\boldsymbol{\sigma}$ we obtain

$$F'\left(\frac{\partial Q}{\partial \sigma_{ij}} + \frac{\partial Q}{\partial q}\frac{\partial f}{\partial \sigma_{ij}}\right) = Q_c'\frac{\partial f}{\partial \sigma_{ij}}. \tag{37}$$

Solving for $\partial f/\partial \boldsymbol{\sigma}$ and substituting the result into eqn (36) we find

$$\frac{\partial \varepsilon_{ij}}{\partial \sigma_{kl}} = \frac{\partial^2 \chi}{\partial \sigma_{ij}\partial \sigma_{kl}} + \frac{F'}{(Q_c' - F'\,\partial Q/\partial q)}\frac{\partial^2 \chi}{\partial \sigma_{ij}\partial q}\frac{\partial^2 \chi}{\partial q\,\partial \sigma_{kl}} \tag{38}$$

where use has been made of definition (25).

In view of the symmetry of eqn (38), we reach the conclusion that nucleation criteria of the type expressed in eqn (24) result in constitutive behavior under monotonic loading which is indiscernible from that of a non-linear elastic material. We have also shown that one can always construct an incremental model of damage such that:

(1) The elastic moduli or, more generally, the Gibbs function exhibit a prespecified dependence on a damage parameter q (e.g. eqns (21)).

(2) It exactly reproduces a prescribed uniaxial tension stress–strain curve (e.g. Fig. 7(a)).

(3) The monotonic stress–strain behavior derives from a potential. This fact is exploited in the analysis that follows.

3.3. *Crack-tip stress intensity factor*

Now consider the asymptotic problem depicted in Fig. 8. It is assumed that the size of the microcracked region is much smaller than the crack length and all other geometrical

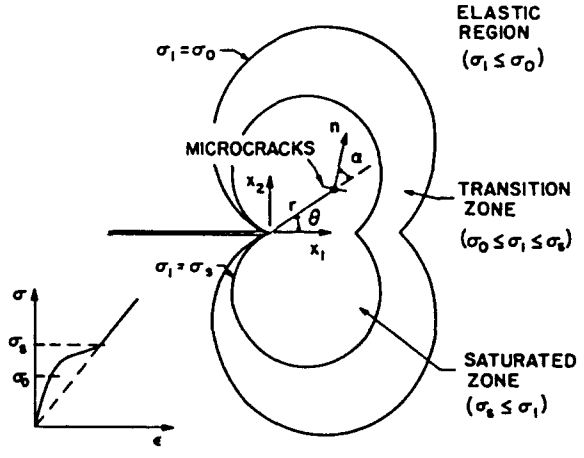

Fig. 8. Small-scale microcracking problem for stationary crack.

dimensions of the body. Under this small-scale damage condition, the crack can be idealized as being semi-infinite. Furthermore, we confine our attention to Mode I loading conditions resulting in symmetric opening of the crack. Three regions can be identified surrounding the crack tip (Fig. 8). In the innermost region the material can be assumed to be saturated. The size of this zone is assumed to be large with respect to the dimensions of the microcracks and their separation and, hence, the microcracked material can be treated as being homogeneous with uniform moduli E_s and ν_s. In the outermost region the material is undamaged and has moduli E_0 and ν_0. Between these two regions lies a transition zone in which the material is partially microcracked.

For the class of materials under consideration the asymptotic stress field can be written as

$$\sigma_{ij}(r,\theta) = \frac{K_t}{\sqrt{(2\pi r)}}\tilde{\sigma}_{ij}(\theta) \tag{39}$$

where (r,θ) is a set of polar coordinates centered at the tip (Fig. 8), K_t is the near-tip stress intensity factor and the angular field $\tilde{\sigma}_{ij}(\theta)$ coincides with the well-known linear isotropic elastic solution (see, e.g. Ref. [20]).

The asymptotic field (39) is assumed to be embedded in a surrounding K-field of the same form but different amplitude K_∞. This latter quantity embodies all information concerning the remotely applied loads as well as the finite geometry of the crack under small-scale microcracking conditions. The ratio K_t/K_∞ is a measure of the extent of shielding of the crack tip by the intervening microcracks, and is the main outcome of the analysis. Under the constitutive restrictions formulated in Section 3.2, the ratio K_t/K_∞ follows readily from an application of the J-integral of Rice[20]. For monotonically increasing K_∞ the stress path undergone by every material point can be expected to be nearly proportional. Under these conditions the material becomes indiscernible from a non-linear elastic material and the J-integral formalism applies. From a remote contour lying entirely within the undamaged region the value of J is computed to be

$$J_\infty = \frac{1-\nu_0^2}{E_0}K_\infty^2. \tag{40}$$

On the other hand, from a contour contained within the saturated region one finds

$$J_t = \frac{1-\nu_s^2}{E_s}K_t^2. \tag{41}$$

By path independence one has $J_t = J_\infty$ and hence

$$\frac{K_t}{K_\infty} = \sqrt{\left(\frac{1-\nu_s^2}{1-\nu_0^2}\,\frac{E_s}{E_0}\right)}. \tag{42}$$

A similar argument has been used by Budiansky *et al.*[22] to prove that transformation toughening is not operative under stationary conditions. A result similar to eqn (33) has been obtained in Ref. [23] under more stringent constitutive restrictions. In the present context, relation (42) is independent of details in the transition from the uncracked to the saturated states. Furthermore, it is not restricted to softening ratios E_s/E_0 close to unity. Unfortunately, the line of reasoning followed above does not carry over to growing cracks since in this case it is no longer possible to assume monotonic stressing throughout the body.

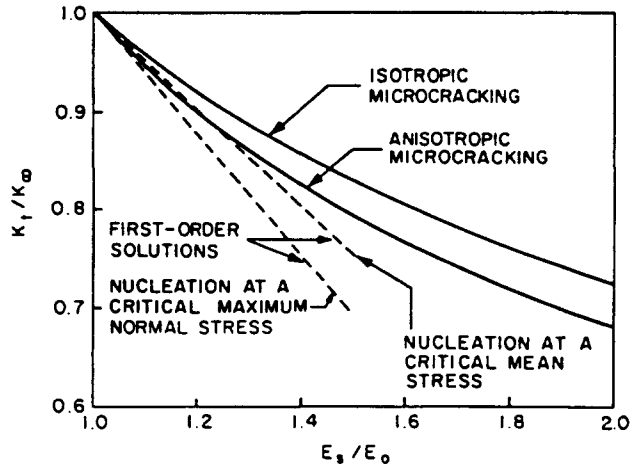

Fig. 9. Reduction in crack tip stress intensity factor due to microcrack shielding.

Figure 9 shows the reduction in the stress intensity factor as a function of the softening ratio E_s/E_0. The value of $(1-\nu_s^2)/(1-\nu_0^2)$ which is required in eqn (42) is obtained from Budiansky and O'Connell's eqns (21) by setting $\bar{E} = E_s$, $\bar{\nu} = \nu_s$ and eliminating the density parameter q. A substantial reduction in stress intensity factor due to microcracking is apparent from Fig. 9. Values of q of about 0.3 at the crack tip have been observed experimentally[24], corresponding to a 30% reduction in K_t. Also in this figure are the results due to Hutchinson[3] for dilute distributions of microcracks and by Ortiz[12] for microcracking normal to the maximum tensile direction. As expected, Hutchinson's first-order formulas agree closely with the results for fully damaged conditions in the limit of small softening ratios E_s/E_0. Furthermore, microcracking normal to the direction of maximum tension is seen to shield the crack tip more effectively than random microcracking, as pointed out by Hutchinson[3].

4. SHIELDING/DAMAGE TRADE-OFF

Two effects of microcracking on fracture toughness have been approximately quantified in previous sections. One weakens the resistance of the material to crack growth while the other delays the onset of macroscopic crack propagation. A question of primary importance is to determine the range of dominance of each effect and under what conditions net toughening is realized. We start by recalling that the size of the cohesive zone within which microcrack coalescence occurs is of the order of a few microcrack lengths and much smaller than the saturated region. Thus, the results derived in Section 2 apply with moduli E and ν given by E_s and ν_s. In particular, it follows that crack growth initiates when

$$\frac{K_t}{K_{IC}^0} = \frac{K_{IC}}{K_{IC}^0} \tag{43}$$

where K_{IC}/K_{IC}^0 is given by eqn (19). In terms of the remotely applied stress intensity factor, condition (43) becomes

$$\frac{K_\infty}{K_{IC}^0} = \frac{K_\infty}{K_t}\frac{K_t}{K_{IC}^0} = \frac{K_\infty}{K_t}\frac{K_{IC}}{K_{IC}^0} = \frac{K_{IC}^{eff}}{K_{IC}^0} \tag{44}$$

where K_t/K_∞ is given by eqn (42). Thus, eqn (44) characterizes the *effective* overall toughness K_{IC}^{eff} of the material as the product of two terms. The first one, $K_\infty/K_t \geqslant 1$, represents the gains derived from shielding, while the second, $K_{IC}/K_{IC}^0 \leqslant 1$ quantifies the losses due to material degradation.

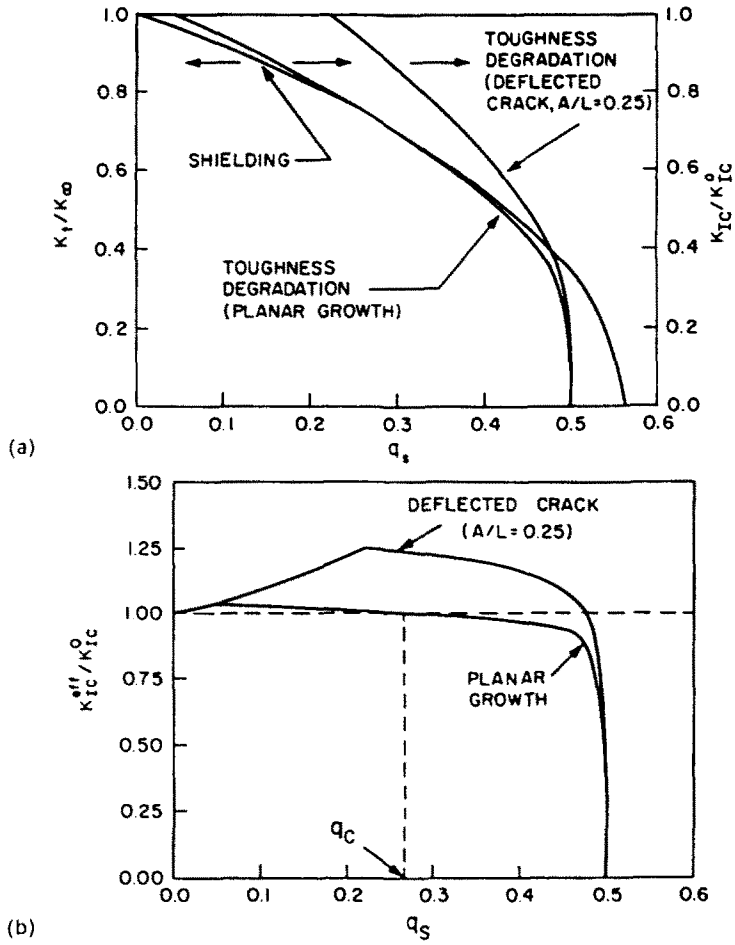

Fig. 10. (a) Comparison of toughness gains and losses due to shielding and material degradation as a function of saturation microcrack density. (b) Net toughening as a function of saturation microcrack density for planar and deflected crack growth.

To make eqn (44) meaningful, it is necessary to establish a relation between the linear microcrack density a_0/l on the plane of the crack and the volumetric microcrack density q_s in the saturated zone. This problem is studied in Appendix B, where the particularly simple relation

$$\frac{a_0}{l} = 2q_s \tag{45}$$

is obtained for planar crack growth. Using this result it is possible to superimpose Figs 5 and 9 and weigh the relative effects of shielding and toughness degradation. The result of this operation is shown in Fig. 10(a), where curves A and B depict the shielding ratio K_I/K_∞ and toughness reduction K_{IC}/K_{IC}^0 as a function of q_s, respectively. The latter dependence is obtained by combining eqns (45) and (19). For a given value of q_s, the dominant mechanism can be readily identified as that corresponding to the uppermost curve.

The most salient feature of this comparison is the fact that, under the assumptions of the present analysis, shielding and toughness degradation seem to counterbalance each other almost exactly. The net toughening of the material is shown in Fig. 10(b) and is seen to be negligible. The balance between both micromechanisms is likely to persist, albeit slightly more favorable to shielding, if the effect of induced anisotropy is taken into account. These observations suggest that other toughening mechanisms need to operate concurrently with microcrack shielding for the experimentally observed toughness enhancement to be obtained. A prime candidate is crack deflection, a mechanism which has not been taken

into account in the analysis given in Section 2. For the materials under consideration, fracture is primarily intergranular[24–28] and the fractured surface exhibits considerable roughness. This has the effect of increasing the area to be cleaved per unit distance advanced by the crack, thus adding to the effective toughness of the material. This feature can be built into the model by suitably modifying the relation between the linear microcrack density a_0/l and the volumetric crack density q_s, as discussed in Appendix B. The resulting shielding/damage trade-off is shown in Fig. 10(a) and the net toughness enhancement in Fig. 10(b). For physically realistic values of the amplitude of the asperities in the cracked surface (e.g. $A/L = 0.25$, eqn (B1)), the extent of toughening is increased by as much as 25% with respect to planar growth. A further beneficial effect of crack deflection is to reduce the effective stress intensity factor acting on the microcracks lying ahead of the main crack. However, the estimates derived by Suresh[29] show that this is a small effect for monolithic ceramics under monotonic loading, with toughness gains of the order of 5%. These factors combined suffice to raise the estimated toughness to levels consistent with the experimental data (see, e.g. Ref. [30]).

The results shown in Fig. 10(b) provide some insight into the effect of grain size on fracture toughness. The propensity for microcracking exhibited by a material appears to be strongly dependent on the grain size[7, 30–32]. Specifically, larger grained materials are observed to be more prone to microfracture than fine grained ones. Thus, the saturation microcrack density q_s can be expected to be a monotonically increasing function of the grain size. Under these conditions, materials with sufficiently small grain sizes will exhibit values of the saturation density $q_s \leqslant q_c$ (Fig. 10(b)) for which microcracking results in net toughening. For coarse grained materials the situation is reversed and net embrittlement becomes the likely outcome of microcracking. These qualitative observations are in agreement with the experimental evidence available to date (see, e.g. Ref. [30]).

Acknowledgements—The support of the Office of Naval Research through grant N00014-85-K-0720 is gratefully acknowledged.

REFERENCES

1. H. Hübner and W. Jillek, Sub-critical crack extension and crack resistance in polycrystalline alumina. *J. Mater. Sci.* **12**, 117–125 (1977).
2. R. Knehans and R. Steinbrech, Memory effect of crack resistance during slow crack growth in notched Al_2O_3 bend specimens. *J. Mater. Sci. Lett.* **1**, 327–329 (1982).
3. J. W. Hutchinson, Crack tip shielding by micro-cracking in brittle solids. Submitted for publication.
4. M. Ortiz and A. Molinari, Microstructural thermal stresses in ceramic materials. *J. Mech. Phys. Solids* (1988), in press.
5. R. G. Hoagland, G. T. Hahn and A. R. Rosenfield, Influence of microstructure on the fracture propagation in rock. *Rock Mech.* **5**, 77–106 (1973).
6. C. C. Wu, S. W. Freiman, R. W. Rice and J. J. Mecholsky, Microstructural aspects of crack propagation in ceramics. *J. Mater. Sci.* **13**, 2659–2670 (1978).
7. Y. Fu, Mechanics of microcrack toughening in ceramics, Ph.D. Dissertation, Department of Materials Science and Mineral Engineering, University of California, Berkeley (Dec. 1983).
8. R. G. Hoagland and J. D. Embury, A treatment of inelastic deformation around a crack tip due to microcracking. *J. Am. Ceram. Soc.* **63**, 404–410 (1980).
9. A. G. Evans and K. T. Faber, Toughening of ceramics by circumferential microcracking. *J. Am. Ceram. Soc.* **64**, 394–398 (1981).
10. Y. Fu and A. G. Evans, Some effects of microcracks on the mechanical properties of brittle solids—I. Stress, strain relations. *Acta Metall.* **33**, 1515–1523 (1985).
11. A. G. Evans and Y. Fu, Some effects of microcracks on the mechanical properties of brittle solids—II. Microcrack toughening. *Acta Metall.* **33**, 1525–1531 (1985).
12. M. Ortiz, A continuum theory of crack shielding in ceramics. *J. Appl. Mech.* **54**, 54–58 (1987).
13. D. S. Dugdale, Yielding of steel sheets containing slits. *J. Mech. Phys. Solids* **8**, 100–104 (1960).
14. G. I. Barenblatt, The mathematical theory of equilibrium of cracks in brittle fracture. *Adv. Appl. Mech.* **7**, 55–129 (1962).
15. B. Budiansky, *Micromechanics II, Proc. 10th Natl Congress of Applied Mechanics* (Edited by J. P. Lamb), pp. 25–32. ASME, Austin (June 1986).
16. D. P. Hasselman, Analysis of the strain at fracture of brittle solids with high densities of microcracks. *J. Am. Ceram. Soc.* **52**, 458–459 (1969).
17. J. P. Singh, C. Shih and D. P. H. Hasselman, Analysis of the effect of crack interaction on nature of strength loss in thermally shocked brittle ceramics. *Commun. Am. Ceram. Soc.* **64**, 106–109 (1981).
18. T. Okada and G. Sines, Crack coalescence and microscopic crack growth in the delayed fracture of alumina. *J. Am. Ceram. Soc.* **66**, 719–725 (1983).

19. W. T. Koiter, An infinite row of collinear cracks in an infinite elastic sheet. *Ingenieur Archiv* **28**, 168–172 (1959).
20. J. R. Rice, Mathematical analysis in the mechanics of fracture. In *Fracture* (Edited by H. Liebowitz), Vol. 2, pp. 191–311. Academic Press, New York (1968).
21. B. Budiansky and R. J. O'Connell, Elastic moduli of a cracked solid. *Int. J. Solids Structures* **12**, 81–97 (1976).
22. B. Budiansky, J. W. Hutchinson and J. C. Lambropoulos, Continuum theory of dilatant transformation toughening in ceramics. *Int. J. Solids Structures* **19**, 337–355 (1983).
23. P. Charalambides and R. M. McMeeking, Near tip mechanics of stress induced microcracking in brittle materials. Submitted for publication.
24. M. Rhüle, A. G. Evans and J. W. Hutchinson, Microcrack toughening in zirconia toughened alumina. Submitted for publication.
25. T. Okada, G. Sines and D. Green, Crack origins and microcracking in the delayed fracture of alumina. *J. Am. Ceram. Soc.* **65**, 64–65 (1982).
26. G. Sines and T. Okada, Identification of flaws responsible for the initiation of slow cracking in the delayed fracture of alumina. *J. Am. Ceram. Soc.* **66**, 228–232 (1983).
27. L. Ewart and S. Suresh, Dynamic fatigue crack growth in polycrystalline alumina under cyclic compression. *J. Mater. Sci. Lett.* **5**, 774–778 (1986).
28. L. Ewart and S. Suresh, Fatigue crack propagation in ceramics. *J. Mater. Sci.* **22**, 1173–1192 (1987).
29. S. Suresh, Fatigue crack deflection and fracture surface contact: micromechanical models. *Metall. Trans.* **16A**, 249–260 (1985).
30. R. W. Rice and S. W. Freiman, Grain-size dependence of fracture energy in ceramics: II, a model for noncubic materials. *J. Am. Ceram. Soc.* **64**, 351–354 (1981).
31. R. W. Rice and R. C. Pohanka, The grain-size dependence of spontaneous cracking in ceramics. *J. Am. Ceram. Soc.* **62**, 559–563 (1979).
32. R. W. Rice, S. W. Frieman and P. S. Becher, Grain-size dependence of fracture energy in ceramics: I. *J. Am. Ceram. Soc.* **64**, 345–350 (1981).

APPENDIX A. J_{IC} FOR A MICROCRACKED SOLID

Equation (15) can be expressed as

$$J_{IC} = \tfrac{1}{2}\sigma_0\delta_0 + \int_{\delta_0}^{\delta_c} \sigma(\delta)\,\mathrm{d}\delta. \tag{A1}$$

At this point it proves convenient to rephrase the integral in eqn (A1) in terms of the microcrack density a/l. Using eqns (4) and (8) with $K_I = K_{IC}^0$ we find

$$\int_{\delta_0}^{\delta_c} \sigma(\delta)\,\mathrm{d}\delta = \frac{1-\nu^2}{E}(K_{IC}^0)^2 \frac{8}{\pi^2}\int_{\theta_0}^{\theta_c} \tilde{\sigma}(\theta)\tilde{\delta}'(\theta)\,\mathrm{d}\theta \tag{A2}$$

where one has

$$\tilde{\sigma}(\theta) = 1\Big/\sqrt{\left(\frac{2}{\pi}\tan\theta\right)}, \quad \tilde{\delta}(\theta) = -\log(\cos\theta)\Big/\sqrt{\left(\frac{2}{\pi}\tan\theta\right)} \tag{A3}$$

in terms of the normalized variables

$$\tilde{\sigma} = \sigma\sqrt{(\pi l)}/K_{IC}^0, \quad \tilde{\delta} = \delta/\alpha l, \quad \theta = \pi a/2l, \quad \alpha = \frac{8}{\pi}\frac{1-\nu^2}{E}\frac{K_{IC}^0}{\sqrt{(\pi l)}}. \tag{A4}$$

In eqn (A2), the upper limit of integration is given by $\theta_c = \pi a_c/2l \approx 1.4295$. The normalized integral in eqn (A2) reduces to

$$\frac{8}{\pi^2}\int_{\theta_0}^{\theta_c} \tilde{\sigma}(\theta)\tilde{\delta}'(\theta)\,\mathrm{d}\theta = \frac{4}{\pi}\int_{\theta_0}^{\theta_c}\left(1 + \frac{\log(\cos\theta)}{2\sin^2\theta}\right)\mathrm{d}\theta \tag{A5}$$

which is readily computed to be

$$\frac{4}{\pi}\int_{\theta_0}^{\theta_c}\left(1 + \frac{\log(\cos\theta)}{2\sin^2\theta}\right)\mathrm{d}\theta = \frac{4}{\pi}\left[\theta - \frac{\log(\cos\theta)}{2\tan\theta} - \arctan\left(\frac{\sin\theta}{\cos\theta+1}\right)\right]_{\theta_0}^{\theta_c}. \tag{A6}$$

Combination of the above equations results in eqn (16), with

$$g(\theta_0) = \frac{4}{\pi}\left[\theta_c - \frac{\log(\cos\theta_c)}{2\tan\theta_c} - \arctan\left(\frac{\sin\theta_c}{\cos\theta_c + 1}\right)\right] - \frac{4}{\pi}\left[\theta_0 - \arctan\left(\frac{\sin\theta_0}{\cos\theta_0 + 1}\right)\right]. \tag{A7}$$

Finally, substituting into (A7) the numerical value of θ_c one obtains the sought result, eqn (17).

APPENDIX B. GEOMETRICAL ESTIMATES OF q AND a/l

Here we concern ourselves with the problem of establishing a correspondence between the volumetric microcrack density $q = N\langle r^3\rangle$ and the linear density a/l on the plane of the main crack. In the materials considered here, fracture is predominantly intergranular[20–24] and the growing crack follows a meandering path. For simplicity, we idealize the deflections w of the fractured surface as exhibiting a doubly sinusoidal profile

$$w(x, y) = A \sin\frac{2\pi x}{L}\sin\frac{2\pi y}{L} \tag{B1}$$

where A and L are the amplitude and period of the tilts, x is the direction of advance of the crack and y the direction of the crack front. The area of the fractured surface per unit area measured on its mean plane is given by

$$\mathscr{A} = \frac{1}{L^2}\int_0^L\int_0^L \left\{1 + \left(\frac{2\pi A}{L}\right)^2\left[\cos^2\frac{2\pi x}{L}\sin^2\frac{2\pi y}{L} + \sin^2\frac{2\pi x}{L}\cos^2\frac{2\pi y}{L}\right]\right\}^{1/2} dx\, dy. \tag{B2}$$

For small amplitudes, this expression is well approximated by

$$\mathscr{A} \approx 1 + \left(\frac{\pi A}{L}\right)^2. \tag{B3}$$

For the physically realistic value $A/L \approx 0.25$, the above expression predicts a 60% increase in the area of the fractured surface with respect to planar growth.

Let M be the number of microcracks per unit area which coalesce with the main crack. Let us idealize these microcracks as being initially circular with a uniform radius r. If all the microcracks under consideration were coplanar, the area to be cleaved per unit area advanced by the crack would be computed to be

$$\mathscr{A}_c = 1 - M\pi r^2. \tag{B4}$$

For irregular growth this area is magnified by eqn (B3), i.e.

$$\mathscr{A}_c = (1 - M\pi r^2)\left[1 + \left(\frac{\pi A}{L}\right)^2\right]. \tag{B5}$$

We determine the initial linear density of microcracks a/l lying ahead of the crack (see Section 2) by matching the area (B4) to be cleaved, which yields

$$\frac{a}{l} = 1 - (1 - M\pi r^2)\left[1 + \left(\frac{\pi A}{L}\right)^2\right]. \tag{B6}$$

For planar growth, this expression reduces to

$$\frac{a}{l} = M\pi r^2. \tag{B7}$$

Next we endeavor to relate M to the volumetric microcrack density. To this end, we assume that the microcracks in M are those which intersect the plane of the crack. Consider all microcracks the center of which lies at a distance z from such a plane. Furthermore, let θ denote the angle made by the plane of a microcrack and the plane of the crack. The intersecting microcracks are those for which $|z| \leqslant r$ and $\theta \geqslant \theta_{min} = a\sin(z/r)$. Under the simplifying assumption that the microcracks are randomly oriented, the number of intersecting microcracks per unit area with centers in the interval $(z, z + dz)$ is given by

$$\mathscr{M}(z)\, dz = \frac{\pi - 2\theta_{min}}{2\pi} N\, dz = \frac{\pi - 2a\sin(z/r)}{2\pi} N\, dz \tag{B8}$$

where N is the number of microcracks per unit volume. Hence, the total number of intersecting microcracks per unit area is computed to be

$$M = \int_{-r}^{r} \mathcal{M}(z)\,dz = \int_{-r}^{r} \frac{\pi - 2a\sin(z/r)}{2\pi} N\,dz = \frac{2}{\pi} Nr. \tag{B9}$$

Substituting the above expression into eqn (B6) we finally find

$$\frac{a}{l} = 1 - (1-2q)\left[1 + \left(\frac{\pi A}{L}\right)^2\right] \tag{B10}$$

where use has been made of the identity $q = Nr^3$. Equation (B10) establishes the sought relation between a/l and q. For planar growth one has $A/L = 0$ and eqn (B10) reduces to the particularly simple expression

$$\frac{a}{l} = 2q. \tag{B11}$$